

Single-Molecule Speckle Analysis of Actin Filament Turnover in Lamellipodia

Naoki Watanabe^{1*} and Timothy J. Mitchison^{1,2}

Lamellipodia are thin, veil-like extensions at the edge of cells that contain a dynamic array of actin filaments. We describe an approach for analyzing spatial regulation of actin polymerization and depolymerization *in vivo* in which we tracked single molecules of actin fused to the green fluorescent protein. Polymerization and the lifetime of actin filaments in lamellipodia were measured with high spatial precision. Basal polymerization and depolymerization occurred throughout lamellipodia with largely constant kinetics, and polymerization was promoted within one micron of the lamellipodium tip. Most of the actin filaments in the lamellipodium were generated by polymerization away from the tip.

Recent studies have opened up the biochemistry underlying the dynamics and structural organization of actin in lamellipodia. Arp2/3

complex plays a key role in actin polymerization, promoting nucleation and dendritic organization of filaments (1, 2). Depolymer-

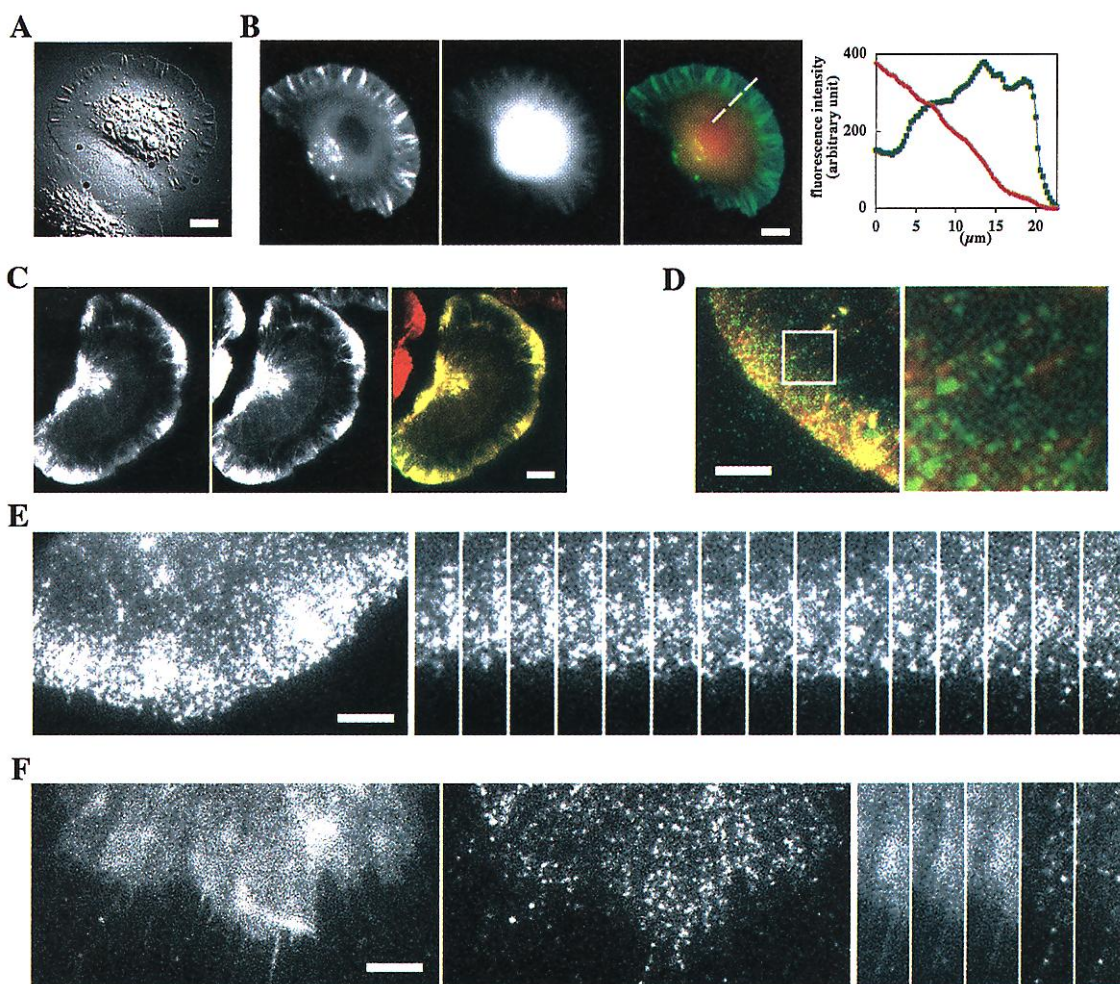
ization is fast, and it may be coupled to polymerization (3). The exact depolymerization mechanism is unknown, but cofilin is thought to play a central role (4). Quantitative modeling of lamellipodium dynamics is a logical goal, but it will require detailed kinetic information on actin dynamics *in vivo*.

Actin dynamics in live cells has been probed by two types of experiments. In time-resolved fixation experiments, incorporation of newly introduced actin subunits into polymers is followed (5, 6). In photoactivation and photobleaching experiments, redistribution of fluorescence fused to actin is followed (7–10). These live-cell studies are supplemented by analysis of actin incorporation after permeabilization (6, 11). These studies highlight the dynamic nature of actin fila-

¹Department of Cell Biology and ²Institute of Chemistry and Cell Biology, Harvard Medical School, 240 Longwood Avenue, Boston, MA 02115, USA.

*To whom correspondence should be addressed. E-mail: naoki_watanabe@hms.harvard.edu

Fig. 1. Distribution of EGFP-actin and the formation of fluorescent speckle images in XTC cells. **(A)** A DIC image of live XTC cells after they were plated onto a poly-L-lysine-coated glass coverslip. **(B)** A live cell coexpressing a high level of EGFP-actin (left) and RFP (middle) and their merged image (EGFP, green; RFP, red) (right). The graph shows fluorescence intensity of EGFP-actin (green) and RFP (red) along the line. **(C)** Distribution of EGFP-actin (left) and Alexa-594 phalloidin (middle) and their merged image (EGFP, green; phalloidin, red) (right) after monomeric actin was extracted (16). **(D)** Speckle images of EGFP-actin (green) and Alexa-594 phalloidin staining (red) in a fixed cell expressing a low level of EGFP-actin. Monomeric actin was extracted as in (C). The indicated area was enlarged at the right. **(E)** Speckle images in a live cell expressing EGFP-actin (left) and its time series acquired at the interval of 4 s (right). On the right, panels show one image every 12 s. **(F)** Untagged EGFP expressed at a low level in a live cell (left) and speckle formation in the same cell after fixation with 2.5% glutaraldehyde (middle). Time series acquired



at the interval of 5 s are shown in the right. The exposure time was constant at 2 s, and fixation was carried out after the third panel (right). Scale bars, 10 μ m.

ments in lamellipodia, but leave important questions unsolved. Subunit incorporation data have been interpreted as showing that polymerization is restricted to the lamellipodium tip (5, 6, 11), whereas photoactivation data have been interpreted as revealing polymerization throughout lamellipodia (8). The data are inadequate to support quantitative modeling because of their limited spatial and temporal resolution. Actin depolymerization rates are probably underestimated by photoactivation and photobleaching experiments because of fast, local reincorporation of disassembled subunits in lamellipodia (12, 13).

To address these deficiencies, we turned to fluorescent speckle imaging (14), in which fluorescent tags incorporated at low concentrations provide fiduciary marks on polymers. To date, speckle analysis has followed clusters of 2 to 10 fluorochromes that happen to lie in the same resolvable unit in the image (15). Because such clusters may include signals from multiple filaments, it has not been possible to directly infer the filament turnover from speckle dynamics. Here, we used more diluted label with endogenous actin (1:10,000 to 1:50,000) (16) and followed speckles of single fluorescent actin molecules.

Xenopus fibroblast (XTC) cells expressing β -actin fused to EGFP (17) were observed soon after being spread onto poly-L-lysine-coated glass coverslips. The enhancer of the cytomegalovirus immediate early promoter (18) in the plasmid was truncated to reduce the expression level (16). XTC cells developed wide lamellipodia firmly attached onto the substrate (Fig. 1A). The thin architecture of lamellipodia, typically $<0.2 \mu\text{m}$ thick (19), was evident from the distribution of untagged red fluorescent proteins (RFP) (Fig. 1B). This allowed us to observe all of the actin in a lamellipodium in a single focal plane. Several observations indicated that EGFP-actin coassembled with cellular actin filaments and provided a nonperturbing probe of actin dynamics. EGFP-actin was efficiently incorporated into actin filament structures without disturbing actin dynamics even when expressed at high levels [Fig. 1B, Web movie 1 (16)]. After monomeric pools were extracted (16), the distribution of EGFP-actin was identical to phalloidin staining (Fig. 1C). EGFP-actin expressed at low levels appeared as speckles that colocalized with actin filament structures (Fig. 1D). These EGFP-actin signals remained tightly associated with actin filaments upon 1 M NaCl extraction, indicating their copolymerization with cellular actin (16). Rearward flow of the bulk actin network was apparent at the same speed of $\sim 1.5 \mu\text{m}/\text{min}$ in cells expressing high and low levels of EGFP-actin [Fig. 1E, Web movies 1 to 3 (16)].

A key aspect of speckle imaging is that only immobilized probes give rise to discrete signals. If the diffusion constant of EGFP-

actin monomer is of the same order as the actin monomer diffusion constant, $\sim 4 \times 10^{-8} \text{ cm}^2/\text{s}$ (20), monomeric probes travel through a path of $>2 \mu\text{m}$ during the 2-s exposure time, and signals will be blurred over many camera pixels. We verified this immobilization requirement by observing time-lapse images of untagged EGFP expressed at a low level in cells, and we compared images before and after fixation (Fig. 1F). Only diffuse signal was observed in live cells, although many speckles appeared after fixation. Because polymerization is the only known mechanism that immobilizes large amounts of actin, EGFP-actin will only give rise to speckles when copolymerized with cellular actin.

To test whether each speckle visualized at very low expression levels consisted of a single EGFP-actin molecule, we tracked ~ 800 individual speckles undergoing photobleaching, using fixed cells to eliminate turnover due to filament disassembly. The kinetics of speckle disappearance matched the prediction that each speckle was a single EGFP-actin molecule (16). The signal decay of individual speckles occurred by a sudden decrease down to background (16), again consistent with the prediction. In live-cell experiments, we restricted our analysis to speckles that had the characteristic signal intensity of single molecules and moved backward at the actin flux rate.

Analysis of single-molecule speckles in live cells was carried out using cells ex-

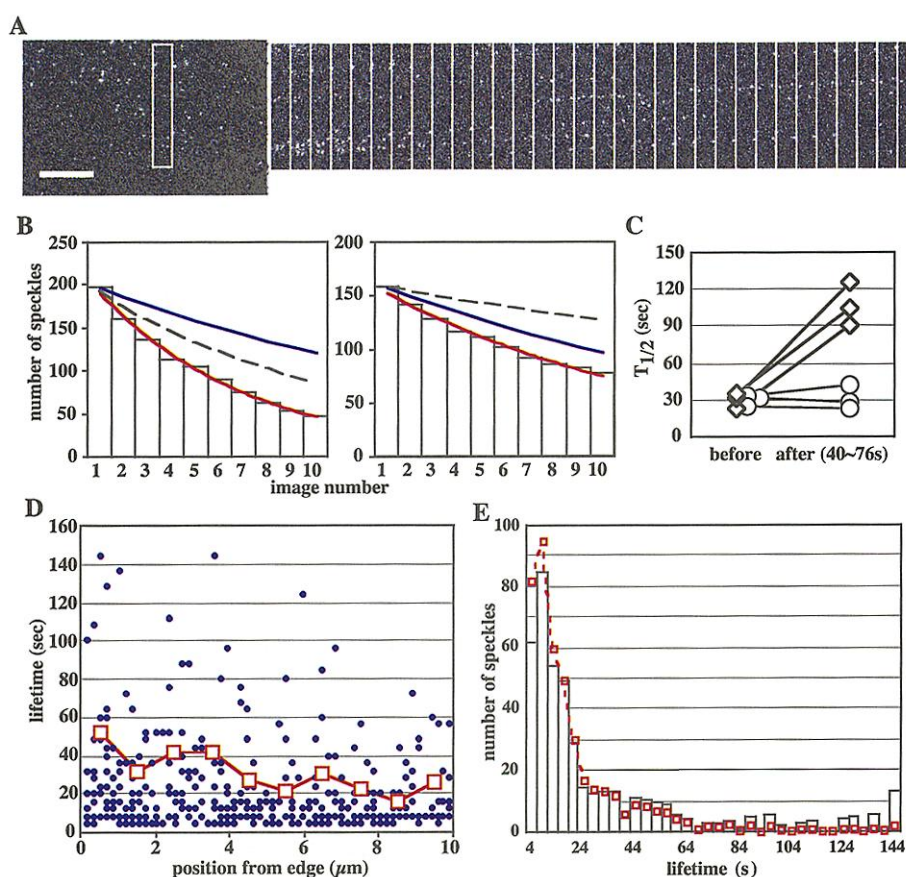


Fig. 2. Actin depolymerization in lamellipodia. (A) A representative speckle image (left) and time series of the indicated area at 4-s intervals (right). Scale bar, $5 \mu\text{m}$. (B) Speckle regression measurements in the same cell before (left) and 40 to 76 s after (right) treatment with $5 \mu\text{M}$ jasplakinolide. Images were acquired at 4-s intervals. Red lines, the best fit single exponential curve for raw data; blue lines, the estimated decay rate due to photobleaching (16); dashed lines, estimated decay due to depolymerization after correction for photobleaching. Before treatment, the ratio of the photobleaching rate to the decay rate of raw data was $\sim 35\%$; after treatment, it increased to $\sim 70\%$. To verify the accuracy of normalization for photobleaching, we carried out regression analysis using less-frequent image acquisition (one per 20 s), and obtained a similar depolymerization rate, $t_{1/2} = 24 \text{ s}$ for untreated cells (16). (C) Change in depolymerization rates in cells treated with $5 \mu\text{M}$ jasplakinolide (connected diamonds) or in cells not treated (connected circles) measured by the regression method. (D) Lifetime versus position plot of speckle lifetime data. Blue dots, the lifetime and emerging position from the cell edge of each speckle; red rectangles, the average speckle lifetime in the indicated area after correction for photobleaching (16). (E) Lifetime distribution in an entire lamellipodium. Red squares, raw data; columns, data normalized for photobleaching (16). Representative results of three measurements are shown (D and E).

pressing very low levels of EGFP-actin [Fig. 2A, Web movie 3 (16)]. We analyzed actin depolymerization by two methods. In the lifetime method, speckles were monitored from their emergence to their disappearance. In the regression method, a set of speckles was identified in one reference image, and the decrease in their numbers

was followed over subsequent images. The regression results were analyzed by approximating with a single exponential curve and correcting for photobleaching (Fig. 2B) (16). This method allowed us to measure rapid change in overall depolymerization rates within a single cell (21). The half-life in lamellipodia averaged 30 s before, and

107 s after, treatment with 5 μM jasplakinolide (Fig. 2C), an actin filament-stabilizing drug (22). That this drug induced stabilization is consistent with our interpretation that disappearance of speckles was due to depolymerization and not blinking of fluorescence (23).

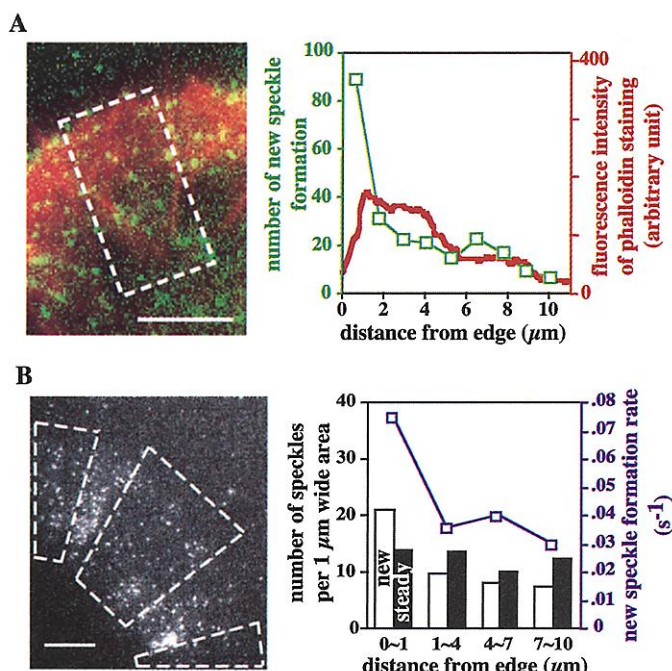
The speckle lifetime method allowed measurement of lifetime distribution of actin filaments. Speckle lifetimes spanned a wide range (4 to 148 sec), regardless of distance from the cell edge (Fig. 2D). The average filament lifetime was almost uniform across the lamellipodium, except for a reproducible 1.3- to 1.6-fold increase in the tip region. The lifetime distribution (Fig. 2E) had several interesting features. First, a large number of subunits (34%) were estimated to depolymerize within 8 s after polymerization, indicating that a lag before the start of depolymerization is of the order of seconds or less. Second, a fraction of subunits had prolonged lifetimes, although the size of this fraction might be inaccurately measured because of photobleaching.

Currently, it is not known how depolymerization starts and proceeds in the filaments. If depolymerization starts solely from pointed ends after Arp2/3 complex (Arp2/3) dissociation (2), our results require an Arp2/3 off-rate of 0.1 to 0.5 per second, faster than a value predictable from the high affinity of Arp2/3 for pointed ends (24). ATP hydrolysis and phosphate release by filaments (25), or by Arp2/3, may promote Arp2/3 dissociation. Alternatively, depolymerization may occur after severing of filaments, catalyzed by cofilin (4) or gelsolin (26). Tropomyosin protects filaments from severing (27) and could account for stabilization of long-lived filaments.

Distribution of polymerization activity was measured by following the appearance of speckles, and comparing it with steady-state filament distribution (Fig. 3). These results revealed two distinct regions of actin polymerization activity. A region within 1 μm of the tip showed higher rates of new speckle formation per unit area than the rest of lamellipodia. In the rest of lamellipodia, new speckles emerged at a rate approximately proportional to the steady-state amount of actin filaments.

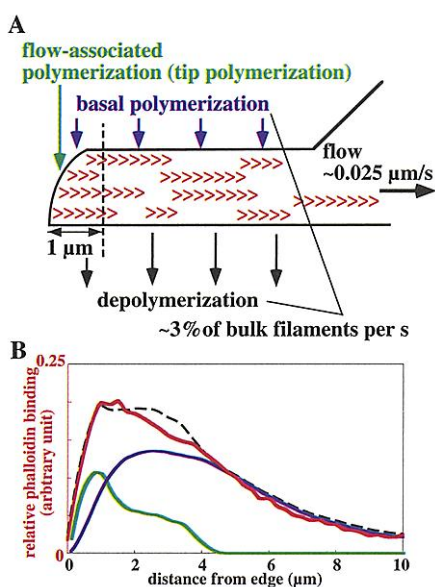
These data are summarized in a phenomenological model (Fig. 4A). In the lamellipodium body, basal polymerization and depolymerization occur with roughly constant kinetics, $\sim 3\%$ of bulk filaments per second. In the tip region, additional polymerization (tip polymerization) is required, because filaments are constantly removed by backward actin flow. We assume that tip polymerization generates the new filament network at a rate proportional to a backward flow rate, 0.025 $\mu\text{m/s}$. Then, the observed high polymerization rates in the tip

Fig. 3. Distribution of actin polymerization activity.



(Left) Actin speckle images used. Emergence of new speckles was followed in the indicated areas (dashed lines) over five consecutive images. Steady-state distribution of total speckles was measured in the third of the five images. [Right (white column)] The number of new speckles formed over 20 s per 1- μm -wide area (N_{new}); (black column), the number of steady-state speckles per 1- μm -wide (N_{steady}); (blue square), new speckle formation rates (s^{-1}). New speckle formation rates were calculated by dividing $N_{\text{new}}/N_{\text{steady}}$ by the sampling interval (20 s). Scale bars, 5 μm .

Fig. 4. Phenomenological model of actin filament dynamics in lamellipodia.



(A) Summary of actin speckle kinetics. Basal polymerization generates and depolymerization disassembles $\sim 3\%$ of the bulk filaments every second throughout the lamellipodium. In addition, polymerization is promoted within 1 μm of the lamellipodium by tip polymerization that generates filaments corresponding to new filament network formation associated with actin backward flow. (B) Quantitative version of the phenomenological model. A representative total filament distribution (red) was obtained by averaging relative intensity of phalloidin staining in eight typical lamellipodia. Using the lifetime distribution (Fig. 2, D and E), a basal polymerization rate of 0.03 s^{-1} of total filaments, and a backward actin flow rate of 0.025 $\mu\text{m/s}$, we modeled the contributions of the two polymerization mechanisms to the steady-state filament distribution (16). Filaments generated by basal polymerization (blue) account for most of the filament distribution in lamellipodia, whereas filaments generated by tip polymerization (green) are predominant only in the tip region. The sum of tip and basal polymers (dashed line) is presented for comparison to the measured filament distribution (red).

region (Fig. 3) could be attributed to the sum of basal and tip polymerization. We modeled relative contribution of tip and basal polymerization to the measured steady-state filament distribution (Fig. 4B). Our results show that polymerization away from the tip generates most of the actin filaments in lamellipodia, consistent with the rapid recovery kinetics of photoactivation experiments (8–10).

These findings will need to be considered in the context of the specific geometric constraints of the leading edge. Tip polymerization might be promoted by factors attached to the lamellipodium tip such as WAVE/Scar, VASP/Mena, and focal adhesion complexes (28–30). Alternatively, tip polymerization could be governed by physical restriction, if the force between the filament end and the plasma membrane regulates filament elongation (31, 32).

Much less is known about how basal polymerization might be regulated, despite its dominant role in determining total filament distribution (Fig. 4B). To accomplish fast basal polymerization, newly growing ends must be continuously generated in the lamellipodium body by some combination of nucleation, severing, uncapping, and shrinking to growing transitions. Such growing ends may affect leading-edge dynamics, extending filaments toward the lamellipodium tip. Potential regulatory mechanisms for basal polymerization include uncapping by phosphoinositides (33) and severing by cofilin (34). Single-molecule analysis of actin regulatory proteins should help determine the role of these pathways and deepen our understanding of the dynamic organization of actin arrays.

References and Notes

1. T. D. Pollard, L. Blanchoin, R. D. Mullins, *Annu. Rev. Biophys. Biomol. Struct.* **29**, 545 (2000).
2. D. Pantaloni, C. Le Clairche, M. F. Carlier, *Science* **292**, 1502 (2001).
3. L. P. Cramer, *Curr. Biol.* **9**, 1095 (1999).
4. J. R. Bamburg, *Annu. Rev. Cell. Dev. Biol.* **15**, 185 (1999).
5. S. Okabe, N. Hirokawa, *J. Cell Biol.* **109**, 1581 (1989).
6. M. H. Symons, T. J. Mitchison, *J. Cell Biol.* **114**, 503 (1991).
7. Y. L. Wang, *J. Cell Biol.* **101**, 597 (1985).
8. J. A. Theriot, T. J. Mitchison, *Nature* **352**, 126 (1991).
9. ———, T. J. Mitchison, *J. Cell Biol.* **119**, 367 (1992).
10. A. Mallavarapu, T. Mitchison, *J. Cell Biol.* **146**, 1097 (1999).
11. M. Bailly *et al.*, *J. Cell Biol.* **145**, 331 (1999).
12. Y. Tardy, J. L. McGrath, J. H. Hartwig, C. F. Dewey, *Biophys. J.* **69**, 1674 (1995).
13. Decay rates of signals marked by photoactivation and photobleaching do not correspond with actin depolymerization rates at fast actin turnover rates (*g*) and at high polymer-to-monomer ratios of actin (Cf:Cm) (72). From high concentration of filaments, ~1000 μM (20), and our observations using the F-actin-preserving extraction method (76), it was estimated that Cf:Cm might exceed 5:1 in lamellipodia. Simulation using the Tardy model (72) estimated that the decay rate of uncaged actin label was about one-half the depolymerization rate at Cf:Cm = 5, *g* = 0.03 (this study), and *D* = 5×10^{-8} cm^2/s (20).
14. C. M. Waterman-Storer, E. D. Salmon, *J. Cell Biol.* **139**, 417 (1997).
15. ———, *Biophys. J.* **75**, 2059 (1998).

16. Supplementary material is available on Science Online at www.sciencemag.org/cgi/content/full/295/5557/1083/DC1
17. C. Ballestrem, B. Wehrle-Haller, B. A. Imhof, *J. Cell Sci.* **111**, 1649 (1998).
18. M. Boshart *et al.*, *Cell* **41**, 521 (1985).
19. V. C. Abraham, V. Krishnamurthi, D. L. Taylor, F. Lanni, *Biophys. J.* **77**, 1721 (1999).
20. J. L. McGrath, Y. Tardy, C. F. Dewey Jr., J. J. Meister, J. H. Hartwig, *Biophys. J.* **75**, 2070 (1998).
21. The lifetime distribution of actin filaments differs from an exponential failure distribution (Fig. 2E), as assumed in photoactivation studies. However, approximating the regression data with a single exponential curve is useful for estimating the overall actin depolymerization rate from a limited number of images (Fig. 2, B and C).
22. M. R. Bubb, I. Spector, B. B. Beyer, K. M. Fosen, *J. Biol. Chem.* **275**, 5163 (2000).
23. R. M. Dickson, A. B. Cubitt, R. Y. Tsien, W. E. Moerner, *Nature* **388**, 355 (1997).
24. R. D. Mullins, J. A. Heuser, T. D. Pollard, *Proc. Natl. Acad. Sci. U.S.A.* **95**, 6181 (1998).

25. L. Blanchoin, T. D. Pollard, R. D. Mullins, *Curr. Biol.* **10**, 1273 (2000).
26. D. J. Kwiatkowski, *Curr. Opin. Cell Biol.* **11**, 103 (1999).
27. S. E. Hitchcock-DeGregori, P. Sampath, T. D. Pollard, *Biochemistry* **27**, 9183 (1988).
28. P. Hahne, A. Sechi, S. Benesch, J. V. Small, *FEBS Lett.* **492**, 215 (2001).
29. H. Nakagawa *et al.*, *J. Cell Sci.* **114**, 1555 (2001).
30. N. A. Hotchin, A. Hall, *J. Cell Biol.* **131**, 1857 (1995).
31. C. S. Peskin, G. M. Odell, G. F. Oster, *Biophys. J.* **65**, 316 (1993).
32. A. Mogilner, G. Oster, *Biophys. J.* **71**, 3030 (1996).
33. J. H. Hartwig *et al.*, *Cell* **82**, 643 (1995).
34. A. Y. Chan, M. Bailly, N. Zebra, J. E. Segall, J. S. Condeelis, *J. Cell Biol.* **148**, 531 (2000).
35. Supported by NIH grant, GM48027, and by Research Fellowship of Uehara Memorial Foundation (N.W.). We thank R. Li and T. Walz for critical reading of the manuscript, and we thank members of the laboratory, especially W. M. Brieher, for helpful discussions.

24 October 2001; accepted 4 January 2002

Generation of an LFA-1 Antagonist by the Transfer of the ICAM-1 Immunoregulatory Epitope to a Small Molecule

T. R. Gadek,^{1*} D. J. Burdick,^{1*} R. S. McDowell,^{1†} M. S. Stanley,¹ J. C. Marsters Jr.,¹ K. J. Paris,¹ D. A. Oare,^{1‡} M. E. Reynolds,¹ C. Ladner,² K. A. Zioncheck,² W. P. Lee,² P. Gribling,² M. S. Dennis,³ N. J. Skelton,³ D. B. Tumas,⁴ K. R. Clark,⁵ S. M. Keating,⁵ M. H. Beresini,⁵ J. W. Tilley,⁶ L. G. Presta,⁷ S. C. Bodary²

The protein-protein interaction between leukocyte functional antigen-1 (LFA-1) and intercellular adhesion molecule-1 (ICAM-1) is critical to lymphocyte and immune system function. Here, we report on the transfer of the contiguous, nonlinear epitope of ICAM-1, responsible for its association with LFA-1, to a small-molecule framework. These LFA-1 antagonists bound LFA-1, blocked binding of ICAM-1, and inhibited a mixed lymphocyte reaction (MLR) with potency significantly greater than that of cyclosporine A. Furthermore, in comparison to an antibody to LFA-1, they exhibited significant anti-inflammatory effects in vivo. These results demonstrate the utility of small-molecule mimics of nonlinear protein epitopes and the protein epitopes themselves as leads in the identification of novel pharmaceutical agents.

The interaction of LFA-1 (the integrin $\alpha\text{L}\beta\text{2}$, CD11a/CD18) with the ICAM proteins 1, 2, and 3 is critical to the adhesion, extravasa-

tion, migration, and proliferation of lymphocytes (1–3). Antibodies directed against the CD11a subunit of LFA-1, which block the binding of its native protein ligand, ICAM-1, have been shown to safely and effectively moderate lymphocyte function in various animal models of human diseases (4–6). Humanized antibodies (7) have been advanced into clinical trials for the treatment of psoriasis and transplant rejection (8, 9). The safety and efficacy observed in these studies has validated LFA-1 as a therapeutic target of interest to the pharmaceutical industry.

An epitope comprising residues E34, K39, M64, Y66, N68, and Q73 (10) within ICAM-1's first domain has been identified as essen-

Departments of ¹Bioorganic Chemistry, ²Immunology, ³Protein Engineering, ⁴Pathology, ⁵Small Molecule Pharmacology, and ⁷Antibody Technology, Genentech, One DNA Way, South San Francisco, CA 94080, USA. ⁶Roche Research Center, Hoffmann-La Roche, Nutley, NJ 07110, USA.

*To whom correspondence should be addressed. E-mail: trg@gene.com (T.R.G.); burdick.dan@gene.com (D.J.B.)

†Present address: Sunesis Pharmaceuticals, 341 Oyster Point Boulevard, South San Francisco, CA 94080, USA.

‡Present address: Gilead Sciences, 333 Lakeside Drive, Foster City, CA 94404, USA.